

Supporting Information

Plasmonic Metal/Mo_xW_{1-x}O_{3-y} for visible-light-enhanced H₂ production from ammonia borane

Haibo Yin,^a Yasutaka Kuwahara,^{ab} Kohsuke Mori,^{abc} Hiromi Yamashita^{ab}

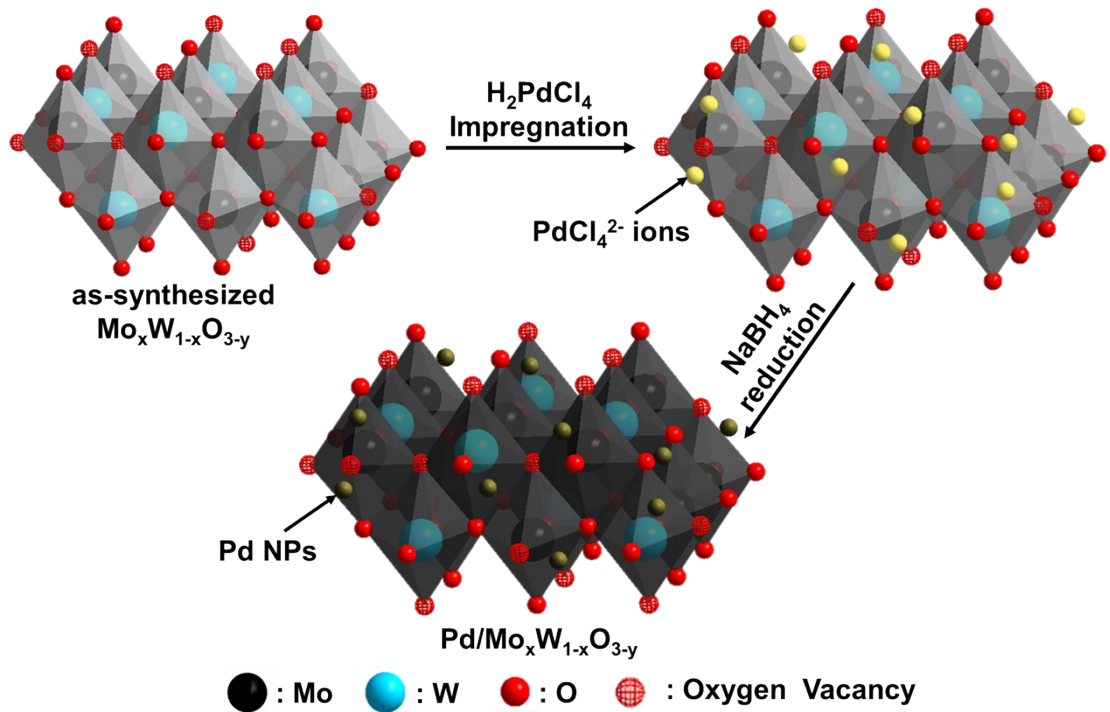
^a Division of Materials and Manufacturing Science, Graduate School of Engineering, Osaka University, Osaka, 565-0871, Japan.

^b Unit of Elements Strategy Initiative for Catalyst & Batteries (ESICB), Kyoto University, Kyoto, 615-8245, Japan.

^c JST, PRESTO, 4-1-8 HonCho, Kawaguchi, Saitama, 332-0012, Japan.

*Corresponding Author

E-mail: yamashita@mat.eng.osaka-u.ac.jp



Scheme S1. Schematic illustration of the synthesis procedure of the $\text{Pd}/\text{Mo}_x\text{W}_{1-x}\text{O}_{3-y}$ hybrid.

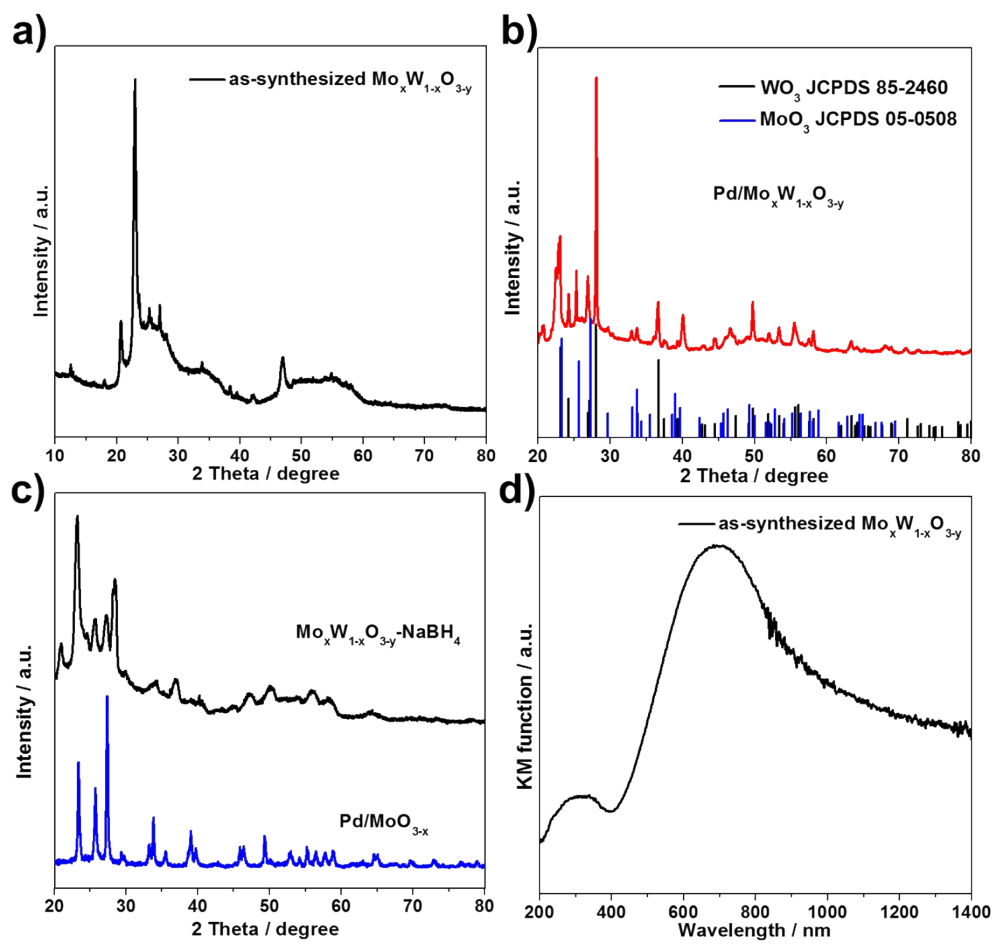


Fig. S1. XRD pattern of a) as-synthesized $\text{Mo}_x\text{W}_{1-x}\text{O}_{3-y}$, b) Pd/ $\text{Mo}_x\text{W}_{1-x}\text{O}_{3-y}$, c) $\text{Mo}_x\text{W}_{1-x}\text{O}_{3-y}\text{-NaBH}_4$ and Pd/ MoO_{3-x} hybrid, respectively. d) UV-Vis-NIR diffuse reflectance spectra of as-synthesized $\text{Mo}_x\text{W}_{1-x}\text{O}_{3-y}$.

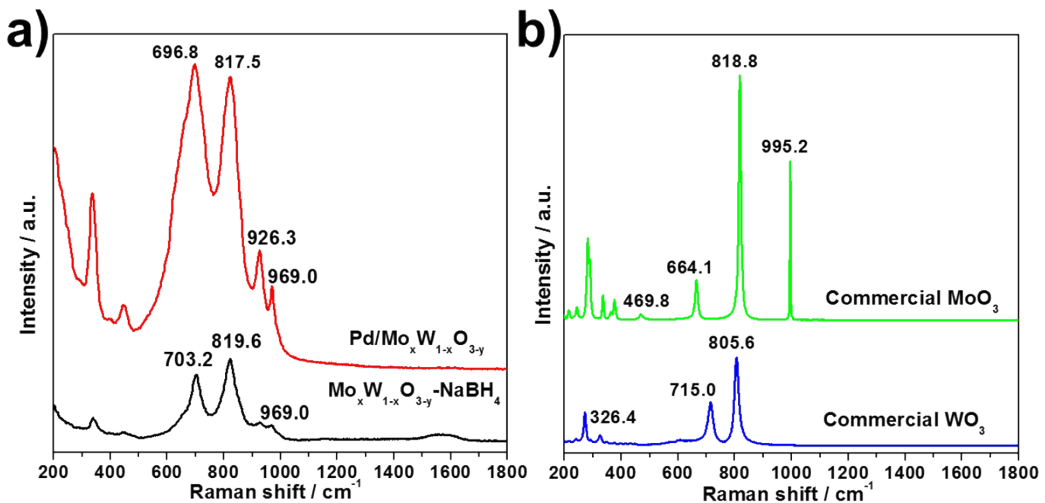


Fig. S2. Raman spectra of a) $\text{Pd}/\text{Mo}_x\text{W}_{1-x}\text{O}_{3-y}$ and $\text{Mo}_x\text{W}_{1-x}\text{O}_{3-y}-\text{NaBH}_4$, b) commercial MoO_3 and commercial WO_3 , respectively.

For commercial MoO_3 , the vibration modes appearing in the frequency ranges of $200-600 \text{ cm}^{-1}$ and $600-1000 \text{ cm}^{-1}$ correspond to the deformation and stretching in Figure S3, respectively. The narrow band at 995 cm^{-1} and the strong band (819 cm^{-1}) are assignable to the antisymmetric ν ($\text{Mo} = \text{O}_1$) and the symmetric ν ($\text{Mo-O}_1\text{-Mo}$) stretching, respectively. The weak and broad bands at 664 and 470 cm^{-1} are ascribable to the antisymmetric ν ($\text{Mo-O}_2\text{-Mo}$) stretching and bending, respectively [1]. For commercial WO_3 , the two main intense peaks at 806 and 715 cm^{-1} correspond to the stretching and bending vibrations of the bridging tungsten and oxygen atoms, which are assigned to the W-O stretching, W-O bending and O-W-O deformation modes, respectively [2].

Table S1. Calculated Mo-O and W-O bond length of commercial MoO_3 , commercial WO_3 , $\text{Mo}_x\text{W}_{1-x}\text{O}_{3-y}$ - NaBH_4 , and Pd/ $\text{Mo}_x\text{W}_{1-x}\text{O}_{3-y}$.

Commercial MoO_3			Commercial WO_3		
Location (cm^{-1})	Mo-O Bond Type	Bond Length (\AA)	Location (cm^{-1})	W-O Bond Type	Bond Length (\AA)
664.15	Equatorial	1.8826	715.09	Equatorial	1.8857
818.87	Apical	1.7815	805.66	Apical	1.8230
995.28	Apical	1.6874			
$\text{Mo}_x\text{W}_{1-x}\text{O}_{3-y}$ - NaBH_4					
Location (cm^{-1})	Mo-O Bond Type	Bond Length (\AA)	Variation (\AA)	W-O Bond Type	Bond Length (\AA)
703.16	Equatorial	1.8550	0.0276	Equatorial	1.8945
819.59	Apical	1.7811	0.0004	Apical	1.7259
969.01	Apical	1.7003	0.0129	--	--
Pd/ $\text{Mo}_x\text{W}_{1-x}\text{O}_{3-y}$					
Location (cm^{-1})	Mo-O Bond Type	Bond Length (\AA)	Variation (\AA)	W-O Bond Type	Bond Length (\AA)
696.88	Equatorial	1.8593	0.0233	Equatorial	1.8993
817.52	Apical	1.7823	0.0008	Apical	1.8153
969.01	Apical	1.7003	0.0129	--	--

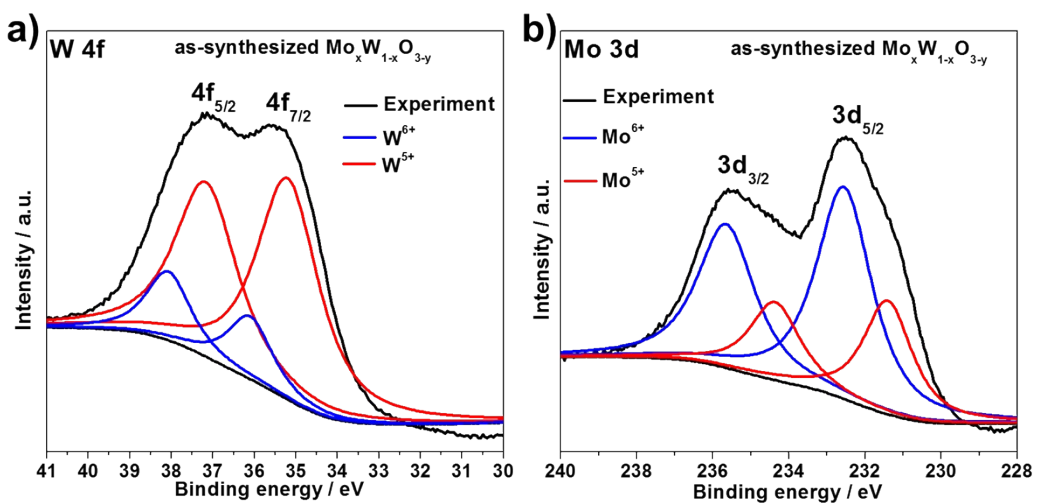


Fig. S3. a) W 4f and b) Mo 3d XPS spectra of as-synthesized $\text{Mo}_x\text{W}_{1-x}\text{O}_{3-y}$.

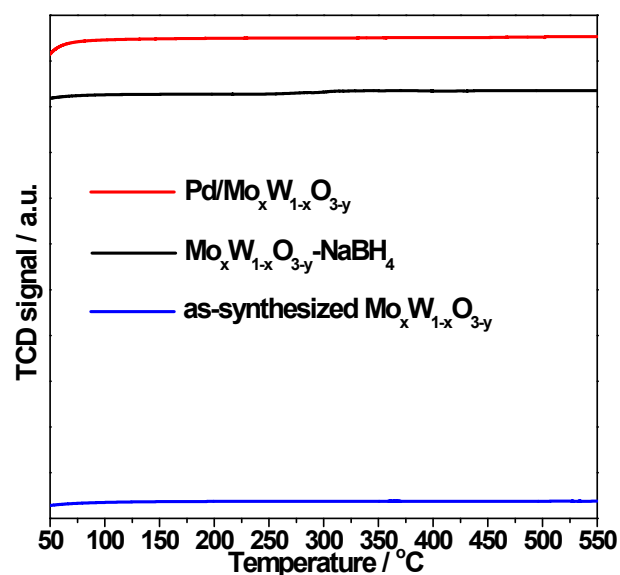


Fig. S4. H_2 TPR plots of Pd/ $\text{Mo}_x\text{W}_{1-x}\text{O}_{3-y}$, $\text{Mo}_x\text{W}_{1-x}\text{O}_{3-y}\text{-NaBH}_4$ and as-synthesized $\text{Mo}_x\text{W}_{1-x}\text{O}_{3-y}$.

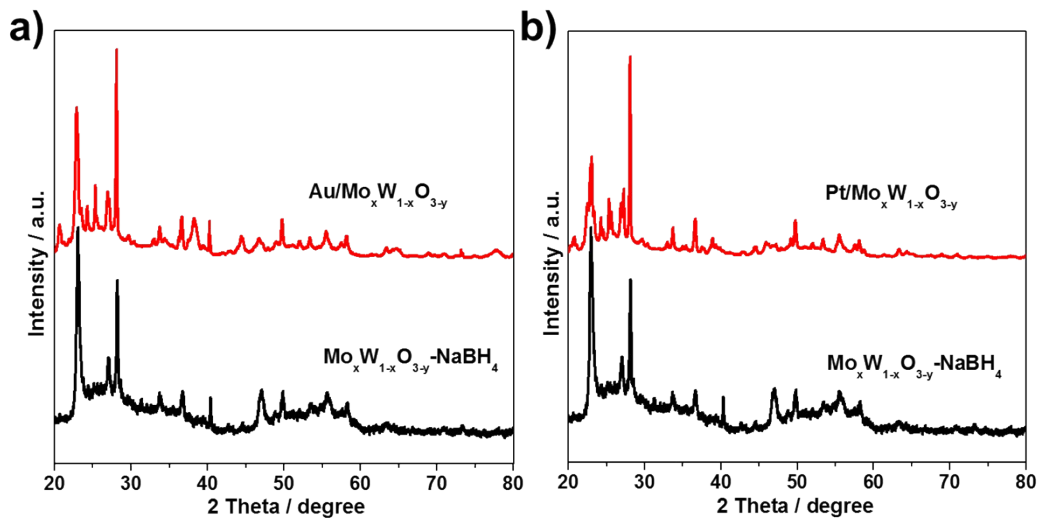


Fig. S5. XRD patterns of a) Au/Mo_xW_{1-x}O_{3-y}, Mo_xW_{1-x}O_{3-y}-NaBH₄, b) Pt/Mo_xW_{1-x}O_{3-y} and Mo_xW_{1-x}O_{3-y}-NaBH₄ hybrid, respectively.

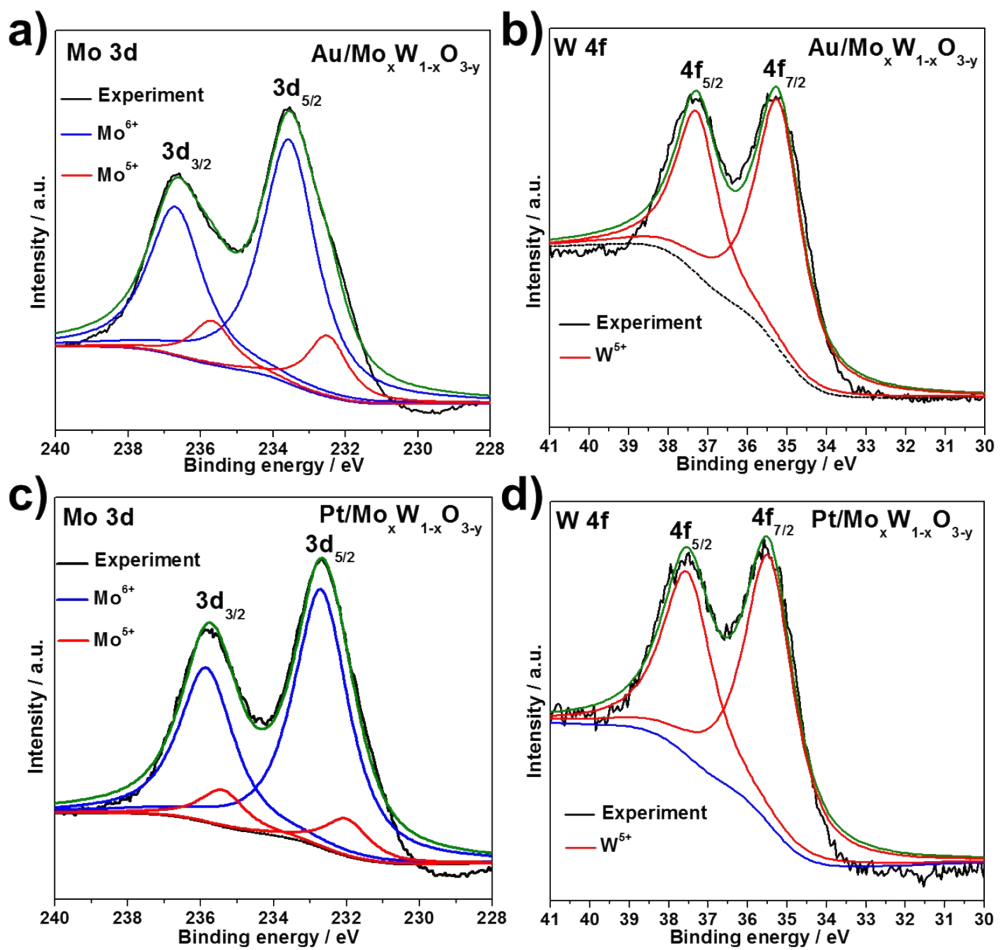


Fig. S6. a) Mo 3d, b) W 4f XPS spectra of the Au/Mo_xW_{1-x}O_{3-y}. c) Mo 3d, b) W 4f XPS spectra of the Pt/Mo_xW_{1-x}O_{3-y}.

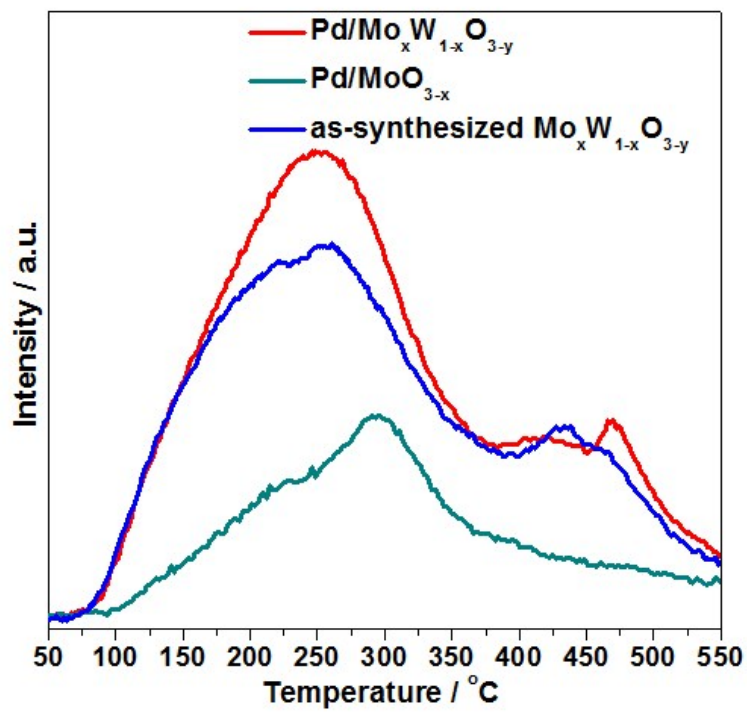


Fig. S7. NH₃-TPD profiles of Pd/Mo_xW_{1-x}O_{3-y}, Pd/MoO_{3-x}, and as-synthesized Mo_xW_{1-x}O_{3-y}.

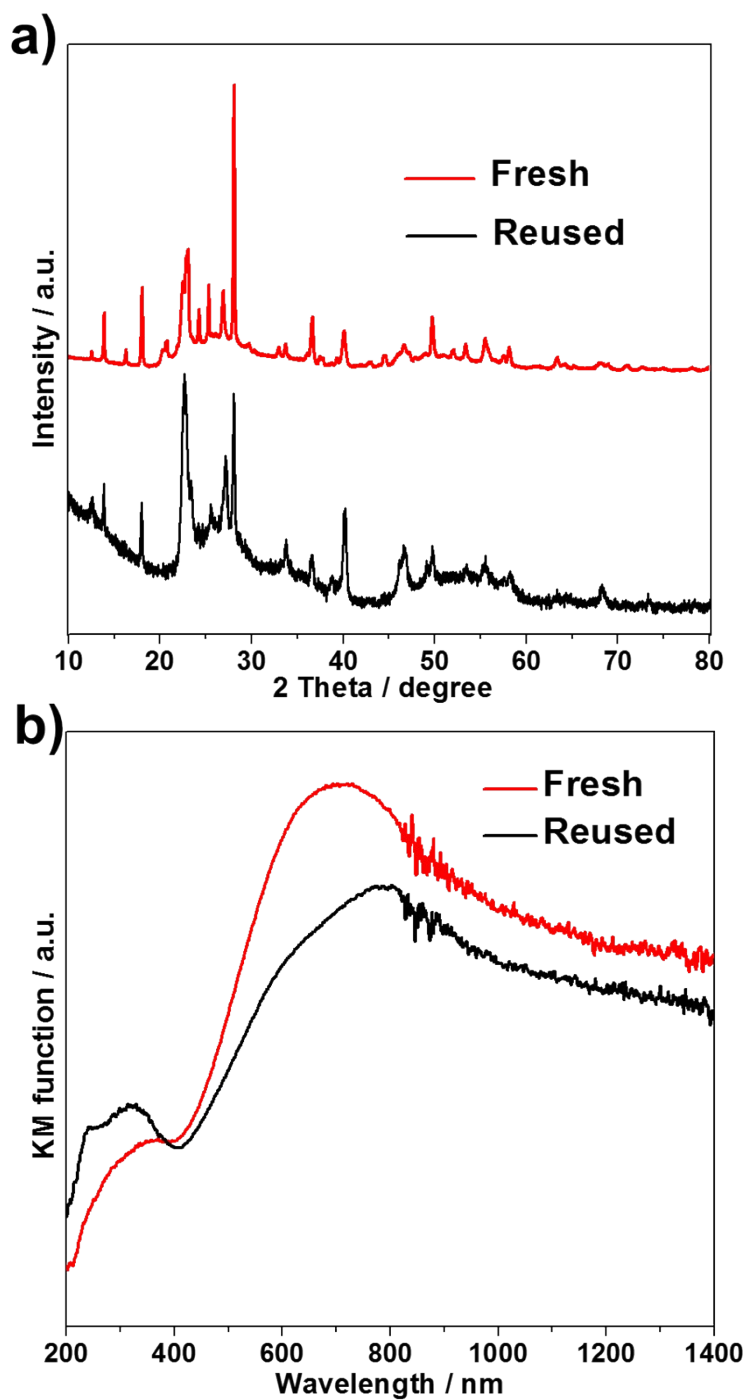


Fig. S8. a) XRD patterns, b) UV-Vis-NIR diffuse reflectance spectra of fresh prepared and reused $\text{Pd}/\text{Mo}_x\text{W}_{1-x}\text{O}_{3-y}$ sample after the recycling NH_3BH_3 dehydrogenation experiments.

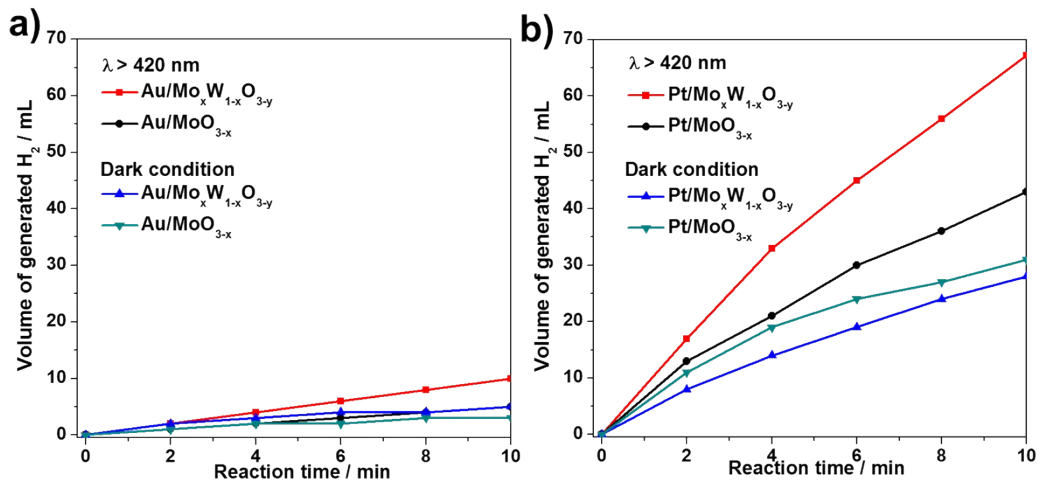


Fig. S9. Comparison of H_2 generation from NH_3BH_3 hydrolysis over a) $\text{Au/Mo}_x\text{W}_{1-x}\text{O}_{3-y}$ and b) $\text{Pt/Mo}_x\text{W}_{1-x}\text{O}_{3-y}$ hybrids.

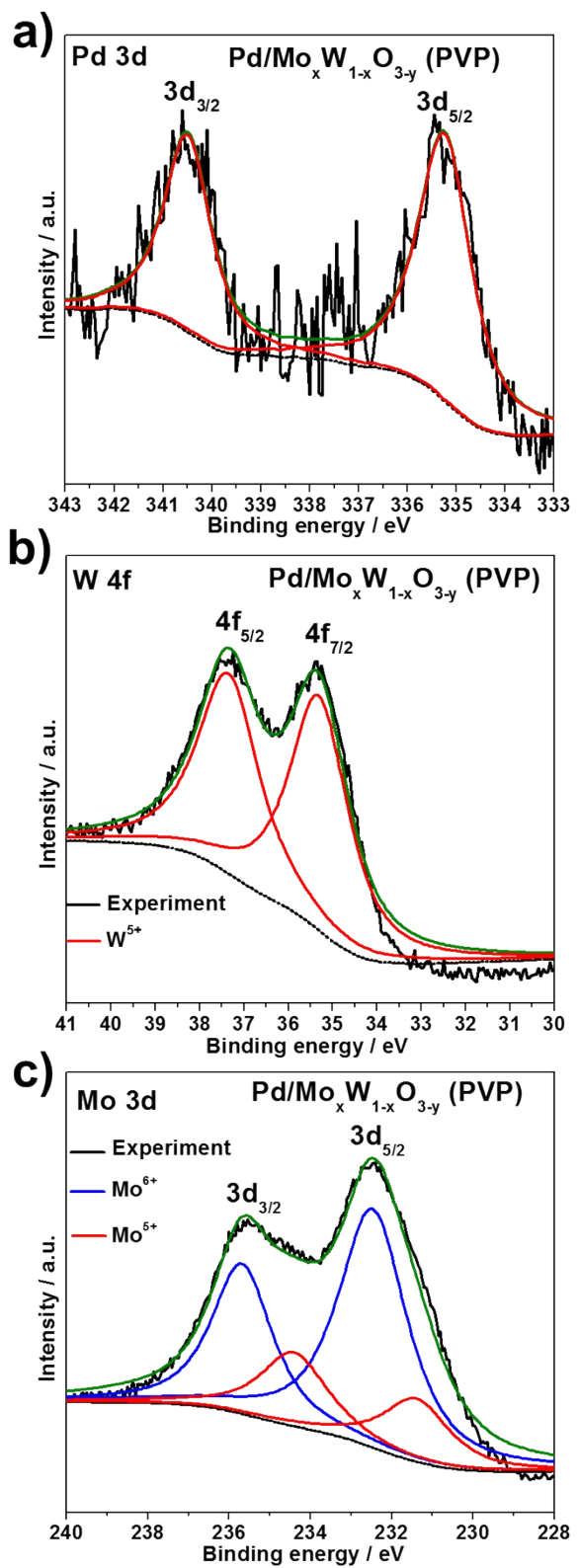


Fig. S10. a) Pd 3d, b) W 4f, c) Mo 3d XPS spectra of the $\text{Pd}/\text{Mo}_x \text{W}_{1-x} \text{O}_{3-y}$ (PVP).

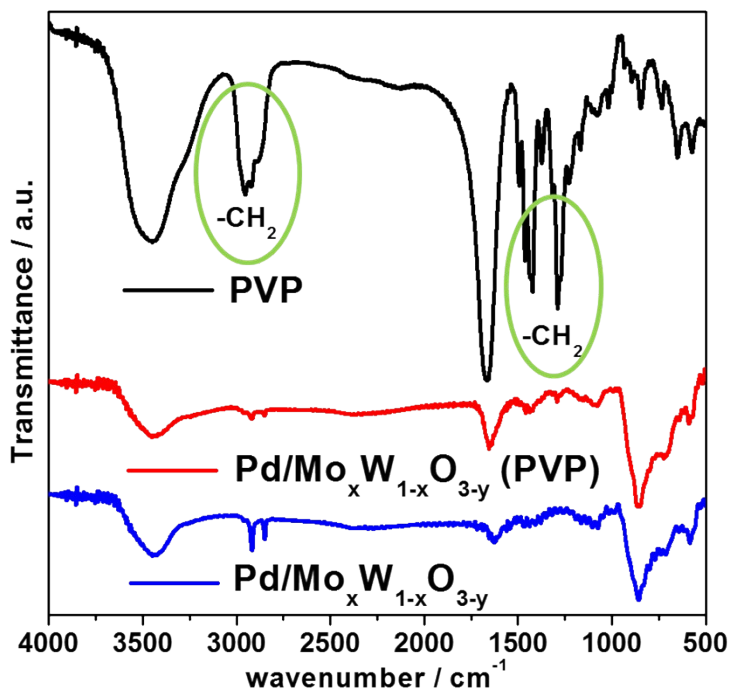


Fig. S11. FT-IR spectra of PVP, $\text{Pd}/\text{Mo}_x\text{W}_{1-x}\text{O}_{3-y}$ hybrids prepared with and without PVP molecules.

- [1] M. Alsaif, K. Latham, M. Field, D. Yao, N. Medehkar, G. Beane, R. Kaner, S. Russo, J. Ou, K. Kalantar-zadeh, *Adv. Mater.* 26 (2014) 3931-3937.
- [2] T. Brezesinski, J. Wang, S. Tolbert, B. Dunn, *Nature Mater.* 9 (2010) 146-151.